Available online at www.sciencedirect.com
ScienceDirect
International Journal of Heat and Mass Transfer 50 (2007) 4915–4926
International Journal of HEAT and MASS TRANSFER
www.elsevier.com/locate/ijhmt

An experimental data set for benchmarking 1-D, transient heat and moisture transfer models of hygroscopic building materials. Part II: Experimental, numerical and analytical data

Prabal Talukdar [a], Olalekan F. Osanyintola [b], Stephen O. Olutimayin [c], Carey J. Simonson [c,*]

[a] Department of Mechanical Engineering, Indian Institute of Technology Delhi, Hauz Khas, New Delhi 110016, India
[b] XXL Engineering Ltd., #101-807 Manning Road NE, Calgary, AB, Canada T2E 7M8
[c] Department of Mechanical Engineering, University of Saskatchewan, 57 Campus Drive, Saskatoon, SK, Canada S7N 5A9

Received 31 March 2006; received in revised form 17 March 2007
Available online 5 June 2007

Abstract

This paper presents the experimental results on spruce plywood and cellulose insulation using the transient moisture transfer (TMT) facility presented in Part I [P. Talukdar, S.O. Olutmayin, O.F. Osanyintola, C.J. Simonson, An experimental data set for benchmarking 1-D, transient heat and moisture transfer models of hygroscopic building materials-Part-I: experimental facility and property data, Int. J. Heat Mass Transfer, in press, doi:10.1016/j.ijheatmasstransfer.2007.03.026] of this paper. The temperature, relative humidity and moisture accumulation distributions within both materials are presented following different and repeated step changes in air humidity and different airflow Reynolds numbers above the materials. The experimental data are compared with numerical data, numerical sensitivity studies and analytical solutions to increase the confidence in the experimental data set.

Keywords: Experimental data; Benchmark; Validation; Heat and moisture transfer; Porous building materials; Spruce plywood; Cellulose insulation

1. Introduction

Heat and moisture transfer in porous media is an important research topic with diverse applications in areas such as, but not limited to: geothermal engineering, building physics [2–8], grain storage [9], textiles [10,11], soil hydrology [12,13], energy conservation and exchangers [14,15], drying technology [16–19], petroleum industry [20], and nuclear waste disposal [21]. While there are numerous journal articles and text books in each application area, one common trend is that many recent works have often focused on numerical and analytical investigations rather than experimental investigations.

The most relevant literatures for this paper are those in building physics and focusing on heat and moisture transfer in porous building materials. Some recent works in this field include advances in integrated simulation tools [22], analytical and numerical methods [23,24] and property measurements [6,25,26]. There is particular interest in heat and moisture transfer between indoor air and hygroscopic building materials during changes in the indoor humidity because there is evidence that this interaction may improve comfort and air quality in buildings [27–29]. In light of this, new experimental data are needed that can be used to accurately quantify heat and moisture transfer between hygroscopic building materials and air with cyclical varying humidity conditions. These data are also important to benchmark models used in this research.

There are experimental data available in the literature that quantifies transient heat and moisture transfer in and between building material and indoor air [22,30–35]. However many of these data sets focus on specific issues such as heat transfer and moisture content as it relates to durability and mould growth, for example, and are not well

* Corresponding author. Tel.: +1 306 966 5479; fax: +1 306 966 5427.
E-mail address: carey.simonson@usask.ca (C.J. Simonson).

0017-9310/$ - see front matter © 2007 Elsevier Ltd. All rights reserved.
doi:10.1016/j.ijheatmasstransfer.2007.03.025

Nomenclature

C_m	moisture storage coefficient
Cp	specific heat capacity at constant pressure [J/(kg K)]
C_1, C_2, ...	constants
D_a	binary diffusion coefficient for water vapor in air [m^2/s]
D_{eff}	effective vapour diffusion coefficient [m^2/s]
D_h	hydraulic diameter [m]
h_a	convective heat transfer coefficient [W m^2 K]
h_m	convective mass transfer coefficient [m/s]
h_{ad}	latent heat of adsorption [J/kg]
h_{fg}	latent heat of vaporization/sorption [J/kg]
k	thermal conductivity [W/(m K)]
$\dot{m}$	rate of phase change [kg/(m^2 s)]
Nu	Nusselt number
P	pressure [Pa]
P_{vsat}	saturated water vapour pressure [Pa]
R	specific gas constant [J/kg K]
Re	Reynolds number of air flow over the specimen
Sh	Sherwood number
t	time [s] or [h] and [day] when specified
T	temperature [K] or [°C] when specified
u	moisture content on a mass basis [kg/kg]
U	moisture accumulation in the sample from the beginning of the test [g]
x	distance from the top of the specimen [m] or [mm] when specified

Greek symbols

$\alpha_{m,eff}$	effective moisture diffusivity [m^2/s]
δ	water vapour permeability [kg/(m s Pa)]
δ_m	vapour boundary layer thickness [m]
ε	volume fraction
ρ	density [kg/m^3]
ρ_0	dry density [kg/m^3]
ϕ	relative humidity in fraction

Subscripts

a	air
eff	effective
g	gas phase (air and water vapour)
i	initial
l	adsorbed phase
s	solid
v	vapour
∞	ambient

suited to benchmark detailed numerical models. Targeted laboratory experiments are often required for model validation. Some experimental data have been measured in carefully planned laboratory experiments [30,33–35] and these can be used for model validation [24,35]. Experiments [30,33,34] were conducted on a bed of fiberglass insulation exposed to warm moist air on one side and a cold impermeable plate on the other side. Following a step change in the cold plate temperature, the temperature and moisture content of the insulation as well as the heat flux at the cold plate were measured and reported. Although these experiments were well controlled and provide important data, the material tested was not very hygroscopic. A majority of the moisture accumulation was due to condensation and frosting near the cold plate. Therefore these data are outside the range of interest for moisture storage in hygroscopic building materials where condensation and frosting are to be avoided, especially in interior walls and furnishings. Furthermore, the cold plate temperature is varied in these experiments, while the air temperature and humidity are kept constant. To benchmark models that intend to consider moisture buffering of hygroscopic materials, experimental data are needed where the air humidity is changed in a transient manner and are presented in this paper. An additional feature of these data is that the humidity profiles within the porous and hygroscopic material are presented, while only moisture content values are presented in Ref. [36]. Ref. [35] also presents similar data for hygroscopic cellulose insulation and this paper expands these data to create more complete data set which complements but does not repeat data in [35].

This paper presents heat and moisture transport through spruce plywood and cellulose insulation. The experimental data for temperature, relative humidity and moisture accumulation within these materials are presented. Experiments are performed with the transient moisture transfer (TMT) facility which is discussed in part I [1] of this paper. All experimental data are compared with results from a model using the material property data presented in [1]. Tests with a single step change in humidity and tests with different flow rates as well as adsorption/desorption cyclical tests (three cycles) are performed for spruce plywood. Similarly, for cellulose insulation, a test with single step change in relative humidity and a 2 day adsorption–desorption test (one cycle) are carried out in addition to a test with different flow rates. Sensitivity studies are performed with the numerical simulation. The effect of a $\pm 10\%$ change in the sorption isotherm, water vapour permeability, heat of sorption, effective thermal conductivity on the temperature and relative humidity is studied for spruce plywood. The moisture storage capacity is presented for spruce plywood and the results of the analytical solution are compared with numerical and experimental results.

2. Experimental data and numerical comparisons

In this section, experimental data are presented for both spruce plywood and cellulose insulation exposed to a range

of transient boundary conditions. To increase confidence in the experimental data and show the expected range of agreement when using the experimental data to benchmark numerical models, the measured temperature, relative humidity and moisture content are directly compared with numerical data obtained with a 1-D heat and moisture transfer model. Comparing numerical and experimental data serves a dual purpose of validating the numerical model as well as confirming that the experimental conditions are well-controlled. The experimental data in this paper are intended to represent one-dimensional, diffusive heat and moisture transport, but in reality there are always some other, although minor, transport phenomena and multi dimensional effects. Comparisons with a one-dimensional diffusive model should reveal the importance of the multi dimensional transport effects. The comparisons will also reveal if all the major experimental uncertainties have been accounted for and systematic errors eliminated.

The governing partial differential equations as well as the thermodynamic constants and boundary condition equations are given in the Appendix. These equations assume that moderate temperature difference exists and that moisture transfer is dominated by vapor diffusion due to water vapor density (or pressure) differences [7,8,37–39].

2.1. Spruce plywood results

Results of three different tests with spruce plywood are presented in this section. The first test is performed with a single step change increase in relative humidity of air flowing above the plywood. The second test is carried out for different Reynolds numbers in the air flow channel above the plywood. The third test consists of a 12 day cyclical test with a step change in relative humidity every 2 days. The test conditions for these tests are given in Table 1. Other tests and results can be found in Ref. [40].

2.1.1. Test with single step change in relative humidity

This test is performed with a single-step change increase in humidity. The plywood is initially conditioned to equilibrium with air at 50% RH ($\phi_i = 50\%$ RH) and the humidity of the air passing over the top of the spruce plywood is 85% RH ($\phi_\infty = 85\%$ RH), giving a nominal humidity change of 35% RH ($\Delta RH = 35\%$). Fig. 1a shows the measured and simulated relative humidity in the plywood at depth of 9 mm and 18 mm in the plywood bed. In Fig. 1 (and all temperature and humidity plots in this paper), the measured value at $x = 9$ mm is the average of 5 sensors located at a depth of 9 mm and the value at $x = 18$ mm is from a single sensor at a depth of 18 mm. It can be seen that it takes about 20 h for the humidity sensor at a depth of 18 mm to begin to record a change in relative humidity. The maximum differences between the experimental and numerical data are 0.35% RH. This agreement is excellent and well within the ±1% RH experimental uncertainty. Relative to the size of the step change in humidity (35%), the measured and simulated data agree within ±1%.

The measured and simulated temperatures at depths of 9 mm and 18 mm are shown Fig. 1b. The agreement between the measured and simulated results is very good, but the maximum change in temperature is very small. Relative to the maximum temperature change during the test (0.25 °C), the experimental and numerical data agree within ±4%. Fig. 1b shows that the temperature in the spruce plywood increases to 23.15 °C at a depth of 9 mm within the first 5 h, which is due to a combination of convection heat transfer from the flowing air and the heat of phase change.

Table 1
Summary of the test conditions used to generate the experimental data

Test description	Initial condition		Condition of air flow			Test duration	Results
	T_i (°C)	ϕ_i (% RH)	T_∞ (°C)	ϕ_∞ (% RH)	*Re*		
Spruce plywood							
Single step change	23	50	23.1	85	2000	2 days	Fig. 1
Test with different flow rates for single step change	22.9	22	23.1	70	1000	2 days	Fig. 2
	23	22	23	70	2000	2 days	
	24	22	24.2	70	4000	2 days	
	24.3	22	24.4	70	7600	2 days	
Adsorption/desorption cyclical test	22	23	23.6/22.8	75/33	2000	12 days	Fig. 3
Sensitivity study tests	23	22	23	70	2000	2 days	Fig. 7 Fig. 8
Comparison with analytical solution	23	22	23	70	2000	2 days	Fig. 9
Cellulose insulation							
Single step change	21	13	21	85	1900	8 h	Fig. 4
Tests with different flow rates for single step change	21	12	21	70	1600	8 h	Fig. 5
	21	12	21	70	1900	8 h	
	21	12	21	70	2100	8 h	
	21	12	21	70	5000	8 h	
Adsorption/desorption cyclical test	21	15	21	70/15	1900	4 days	Fig. 6

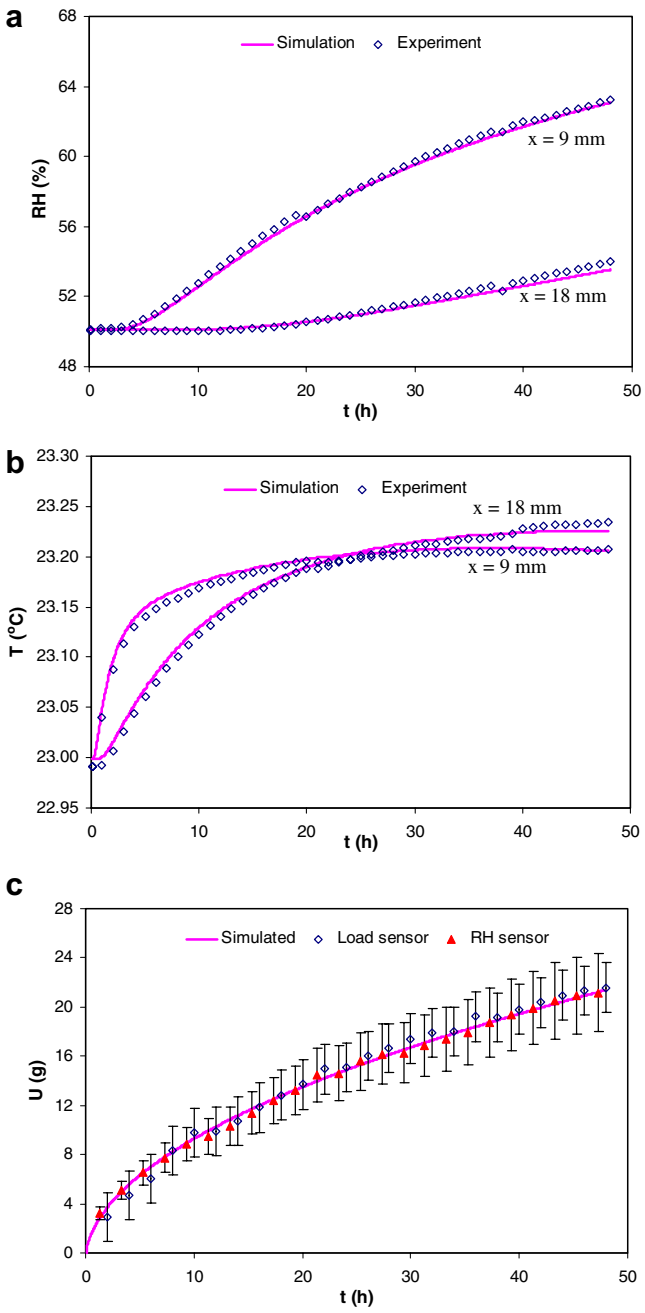

Fig. 1. Measured and simulated (a) relative humidity, (b) temperature and (c) moisture accumulation within the plywood bed following a 35% RH step change.

After about 22 h, the temperature of the plywood at $x = 18$ mm exceeds the temperature at $x = 9$ mm due to the diffusion of heat into the plywood and convection heat transfer to the air above the plywood. The thermal boundary layer grows faster than the vapour boundary layer as can be seen by comparing Fig. 1a and b. The thermal boundary layer penetrates to a depth of 18 mm after the first hour, while the water vapour boundary layer does not penetrate to a depth of 18 mm until after 20 h.

Fig. 1c presents a comparison between the moisture accumulation calculated with the numerical model and that measured using load sensors and the relative humidity sensors in the airstream. All data show that the rate of moisture accumulation decreases with time as expected. The maximum differences between the measured and simulated moisture accumulation is 1.3 g for the load sensors and 1.9 g for the relative humidity sensors, respectively, and both are well within the experimental uncertainty bounds as shown in Fig. 1c.

2.1.2. Test with different flow rates

This section presents results of tests using four different airflow rates, which corresponds to Reynolds numbers of 1000, 2000, 4000 and 7600. The purpose of this test is to investigate the effect of the convective heat and mass transfer coefficients on the temperature and relative humidity fields, and the results are presented in Fig. 2.

Fig. 2a and c shows that the relative humidity and moisture accumulation increases as Re increases, which is expected because as Re increases, the convective heat and mass transfer coefficients increase [47,48] and thus moisture accumulation and relative humidity within the plywood increase. The measured temperatures at $Re = 4000$ and 7600 are significantly different than the values at $Re = 1000$ and 2000 as shown in Fig. 2b. This is because of the different air temperatures (T_∞) in the tests with higher flow rates as shown in Table 1.

When using the experimental boundary conditions specified in Table 1 in the numerical model, the numerical and experimental results are in close agreement. The maximum differences between the measured and simulated relative humidity, temperature and moisture accumulation using the load sensors are 0.7%, 4% and 6% for the laminar flow tests ($Re = 1000$ and 2000) and 1.1%, 20% and 10% for the turbulent flow tests ($Re = 4000$ and 7600) when normalized by the maximum change in the measured relative humidity, temperature and moisture accumulation, respectively.

2.1.3. Adsorption/desorption cyclical test

In this test, the plywood, initially at equilibrium with air at 22% RH and 23 °C, is tested for 12 days in the TMT facility with $Re = 2000$. During this time, the plywood is subjected to 6 step changes in humidity each 2 days apart. The average conditions of the air flowing over the plywood are 75% RH and 23.6 °C during the adsorption phase of the humidity cycle and 33% RH and 22.8 °C during the desorption phase. The measured and simulated relative humidity and moisture accumulation within the spruce plywood for the adsorption–desorption cyclical test are shown in Fig. 3. The maximum differences between the measured and simulated data are 0.7% for relative humidity and 6% (load sensors) and 11% (relative humidity sensors) for moisture accumulation when normalized by the maximum change in relative humidity and moisture accumulation. These differences indicate a range of acceptable agreement between the model and experiments, which are in the same order as the experimental uncertainty [1], for an adsorption–desorption cycle that has a 2 day adsorption phase

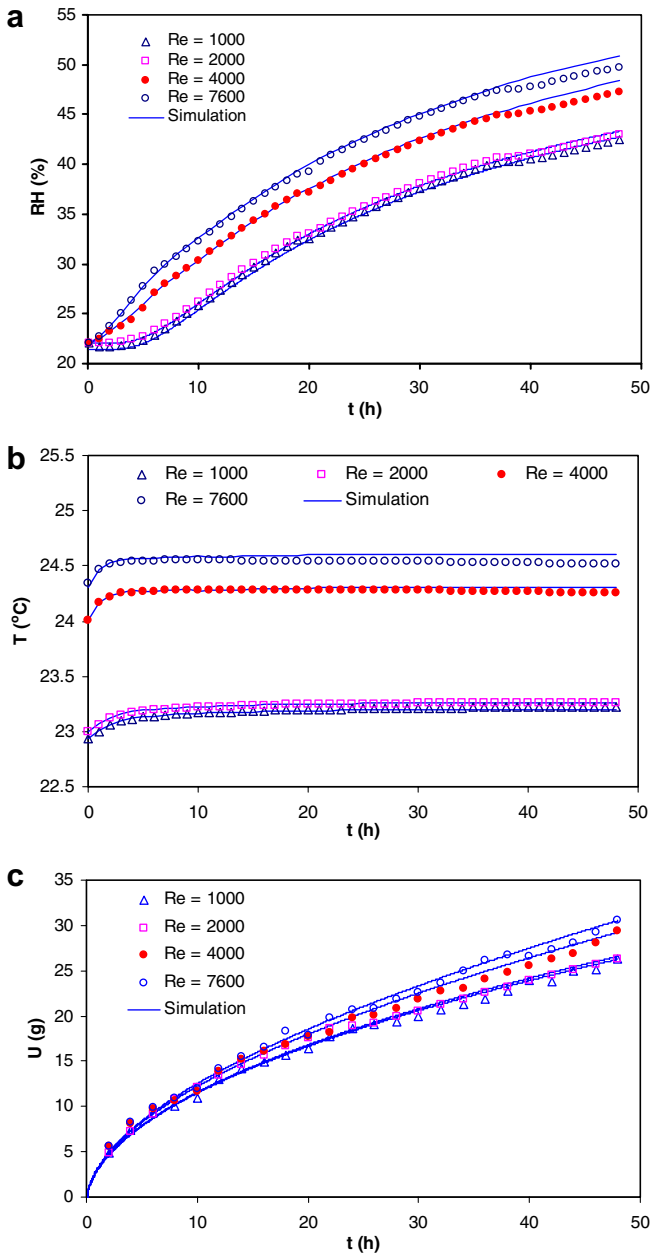

Fig. 2. Measured and simulated (a) relative humidity, (b) temperature and (c) moisture accumulation within the plywood at a depth of 9 mm following a 50% RH step change with different airflow rates.

followed by a 2 day desorption phase. Moisture accumulation data for a shorter adsorption–desorption cycle consisting of 8 h of adsorption followed by 16 h of desorption can be found in Refs. [36,40].

2.2. Cellulose insulation results

Results of three different tests with cellulose insulation are presented in this section. The first test is an isothermal test with the air flowing over the cellulose bed is at a higher humidity of 85% RH while the bed is at an initial humidity of 13% RH. The second test is carried out with different air-

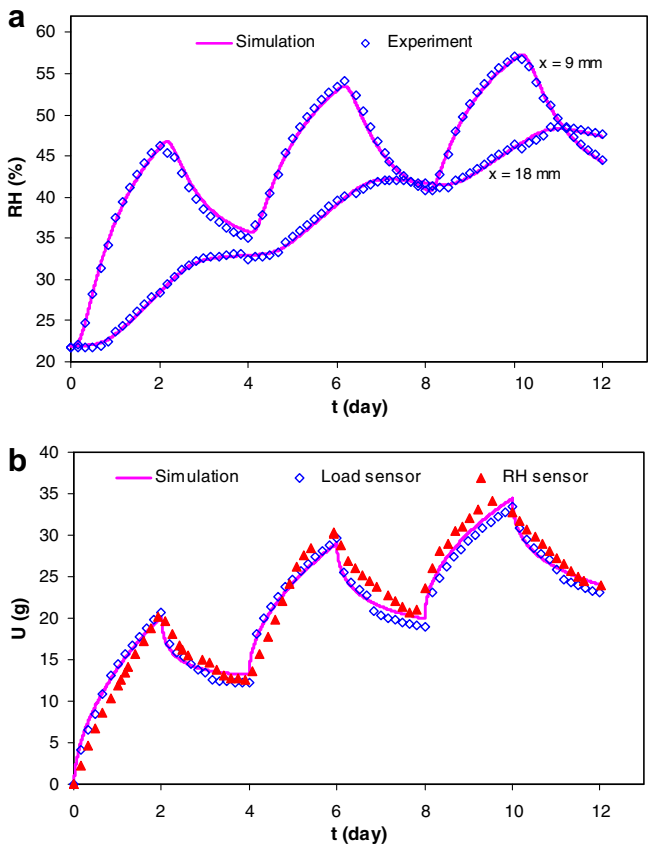

Fig. 3. Measured and simulated (a) relative humidity and (b) moisture accumulation within the plywood during the cyclical adsorption/desorption test.

flow rates to see its effect on temperature and relative humidity in the bed. In the third test, a wetting and drying test is conducted using two different air humidities (70% RH and 15% RH) over a span of 2 days. These test conditions are summarized in Table 1. Other tests and results can be found in Ref. [41].

2.2.1. Test with single step change in relative humidity

In this test, the cellulose insulation bed is at initial conditions of 13% RH and 21 °C and the air passing over the top surface of the insulation bed is at 85% RH, 21 °C and $Re = 1900$. This is the largest step change investigated in this paper and larger than isothermal step change investigated by Olutimayin and Simonson [35] and the repeatability test in part I [1] of this paper. The vapor density of the air passing over the top surface for this test is 0.0156 kg/m^3, while that in [1,35] is 0.0128 kg/m^3 ($\phi_\infty = 70\%$ RH and $T_\infty = 21$ °C). The test in this paper with $\phi_\infty = 85\%$ RH has 22% higher vapor density than the isothermal test with $\phi_\infty = 70\%$ RH; hence an increase in vapor penetration is expected for this test compared to the data in [1,35].

Fig. 4a shows the measured and simulated relative humidity in the medium for a test period of 8 h. The increase in relative humidity at a depth of 60 mm is 20% RH after 8 h which is 14% greater than the 17.5% RH

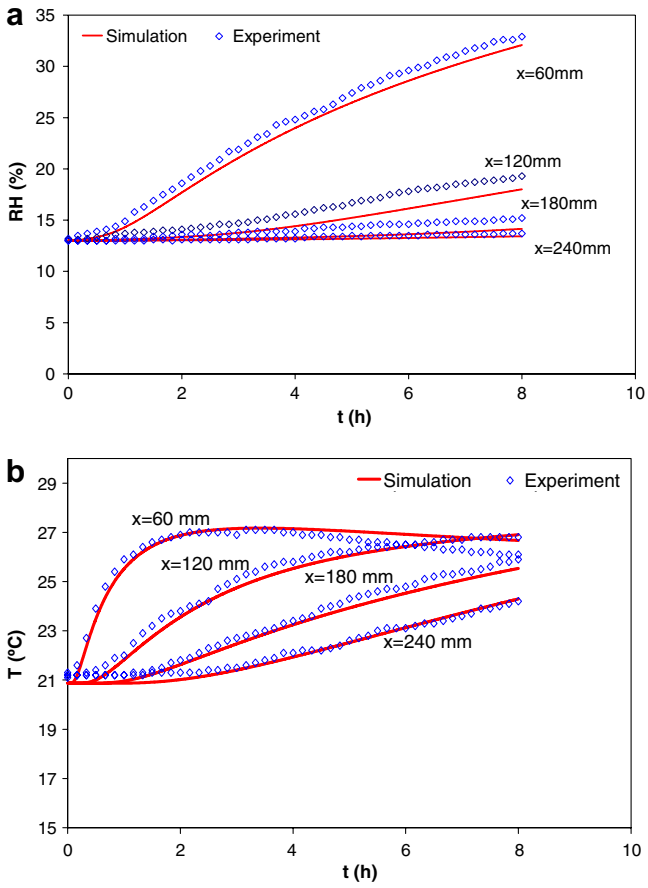

Fig. 4. Measured and simulated (a) relative humidity and (b) temperature within the cellulose insulation bed following a step increase in air humidity from 13% RH to 85% RH.

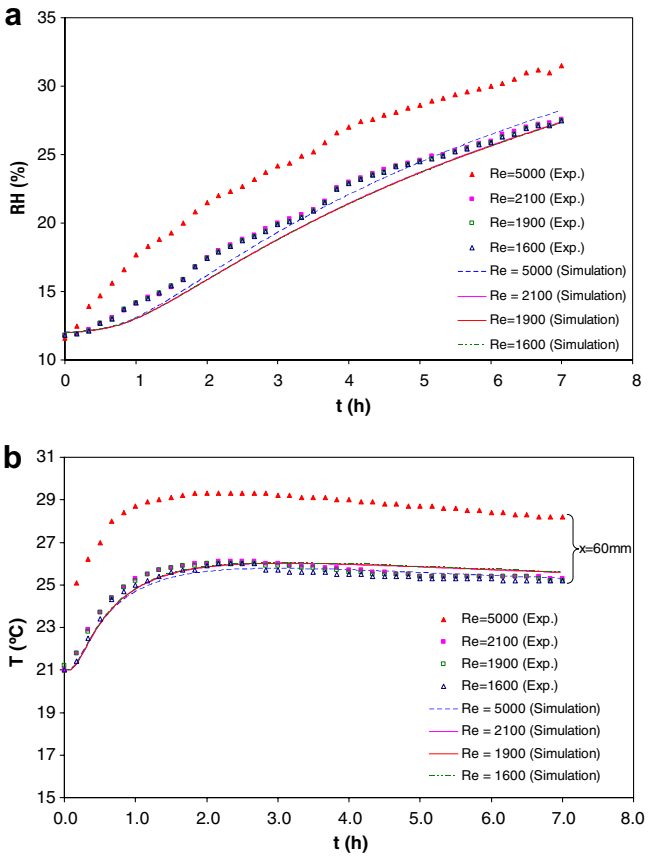

Fig. 5. Measured and simulated (a) relative humidity and (b) temperature in the cellulose insulation bed at $x = 60$ mm for tests with different airflow rates.

increase when $\phi_\infty = 70\%$ RH [1,35]. This increase in relative humidity for the isothermal test with air conditions at 85% RH and 21 °C is in good agreement with the expected results. The maximum and average differences between the experimental data and numerical simulation are 0.8% RH and 0.3% RH respectively, showing excellent agreement between the experimental and numerical results.

The measured and simulated temperatures in the medium are shown in Fig. 4b. As with the plywood results, the thermal boundary layer grows faster than the vapor boundary layer. The temperature in the medium at a depth of 60 mm rose by 6 °C after 2 h of testing, which is 1 °C larger increase compared to the increase in temperature at the same time and location for the isothermal test with air at 70% RH [35]. This increase in temperature is due to the increase in moisture adsorbed and thus an increase in heat release during the test with $\phi_\infty = 85\%$ RH. The maximum and average differences between the measured and simulated temperatures are 0.4 °C and 0.2 °C respectively.

2.2.2. Test with different flow rates

Four different airflow rates are used in these tests, corresponding to Reynolds numbers of 1600, 1900, 2100 and 5000. For these tests, the cellulose insulation is at initial conditions of 12% RH and 21 °C. Air at 70% RH and 21 °C is passed over the top surface of the insulation bed. To directly compare the results at different airflow rates, the measured relative humidity and temperature at $x = 60$ mm from the top of the bed are presented in Fig. 5. In the case of laminar flow ($Re = 1600$, 1900 and 2100), the effect of Re is very minor. It is indistinguishable in the simulation data and just noticeable in the experimental data. The maximum difference between measured and simulated relative humidity for the laminar flow tests ($Re = 1600$, 1900 and 2100) is 1.6% RH. However, the maximum difference between the measured and simulated relative humidity for the turbulent flow test ($Re = 5000$) is 4.7% RH. This difference is larger than the uncertainty of the humidity sensors and the expected repeatability of the experiment and is likely due to airflow through the insulation as discussed in part I [1] of this paper. The flow of moist air through the insulation will increase the humidity in the insulation compared to pure diffusion and therefore the measured relative humidities exceed the simulated values at $Re = 5000$. The same trend can be seen in the temperature plots where the agreement between the measured and simulated data is good for the laminar flow cases, but not for the turbulent flow case. Modeling the two-dimensional heat and moisture equations including advec-

tion are outside the scope of the current study and are left for future work.

2.2.3. Adsorption/desorption cyclical test

For this test, the initial conditions in the cellulose insulation bed are 15% RH and 21 °C. Air at 70% RH and 21 °C is passed over the top surface of the insulation for 2 days. After this period, the conditions of the air passing over the top surface are reverted to the initial conditions of 15% RH and 21 °C for another two days. The Reynolds number for the airflow is 1900.

The measured and simulated relative humidities in the cellulose insulation bed for the wetting and drying test are shown in Fig. 6a. The measured relative humidity shows a very good agreement with the simulated values for the wetting process (within ±1.5% RH). However, for the upper portion of the cellulose insulation bed (which is the most active portion for moisture transfer), the measured values show a poorer agreement with the simulated values during the drying process (within ±3% RH). For the other 2 locations at $x = 120$ and 180 mm, the maximum and average difference between the measured and simulated values are around 3% RH and 2% RH, respectively. The differences between the measured and simulated data indicate a range of acceptable agreement when using these data for benchmarking numerical models.

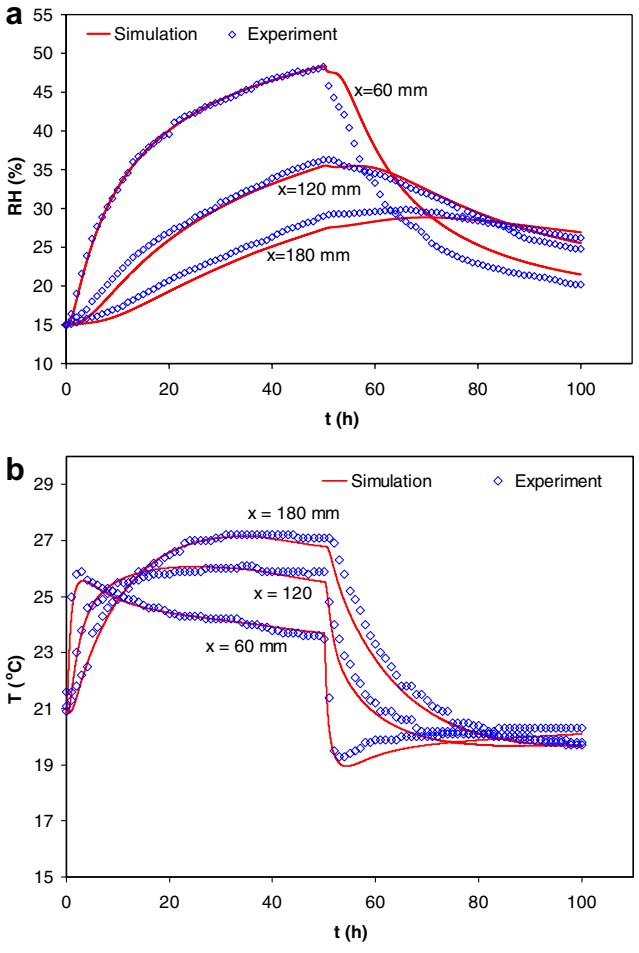

Fig. 6. Measured and simulated (a) relative humidity and (b) temperature in the cellulose insulation bed for the adsorption/desorption test.

Fig. 6b shows the measured and simulated temperatures in the cellulose insulation medium for the adsorption/desorption test. The maximum and average differences between the measured and simulated temperatures in the medium are 0.7 °C and 0.3 °C for the entire wetting and drying tests. The temperature in the medium at the end of the drying process is lower than the initial temperature in the medium at the start of the wetting process. For example, the measured and simulated temperatures in the cellulose insulation bed at the end of the drying process are 20 °C and 19.7 °C respectively at a depth of 180 mm in the cellulose insulation bed, which are lower than the initial temperature at the start of the wetting process (21 °C) which is due to the energy required for the desorption of water from the cellulose.

2. Sensitivity studies of spruce plywood

The sensitivity of the numerical results to changes in the sorption isotherm, effective thermal conductivity, heat of sorption and effective diffusion coefficient are presented in this section. These studies are important because inter laboratory comparisons of thermal and moisture properties of building materials show that significant variations often exists [26,42]. A ±10% variation in each material property for plywood [1] will be studied independently to show the possible deviation in the numerical results due to changes in the properties. A sensitivity study is not performed for cellulose insulation because a similar study can be found in [35]. All the sensitivity studies are performed using the 50% RH single-step change test conditions at $Re = 2000$ (Table 1). The results of the sensitivity studies are concentrated on the locations in the spruce plywood where the numerical results were verified with experimental data; these locations are 9 mm and 18 mm for the relative humidity data and only 9 mm for the temperature for clarity.

Fig. 7a shows that increasing the sorption curve by 10% results in a 6% reduction in the humidity, relative to the size of the step change in humidity (50%), at $x = 9$ mm and $t = 48$ h, whereas, a 10% reduction in the sorption curve increases the relative humidity by a maximum of 6% at $x = 9$ mm and $t = 48$ h. For the simulated temperature presented in Fig. 7b, a 10% increase in the sorption curve increases the temperature by up to 10%, while a 10% reduction in the sorption curve decreases the temperature by up to 10%. These results make physical sense because an increase in the sorption isotherm will mean more moisture accumulation, which will reduce the water vapour diffusion within the vapour phase and thus reduce the relative humidity as well as increase the temperature due to the phase change. These results help confirm the sorption curve used in the model and presented in part I [1] of this paper because the differences between the measured and simulated relative humidities (Figs. 1–6) are typ-

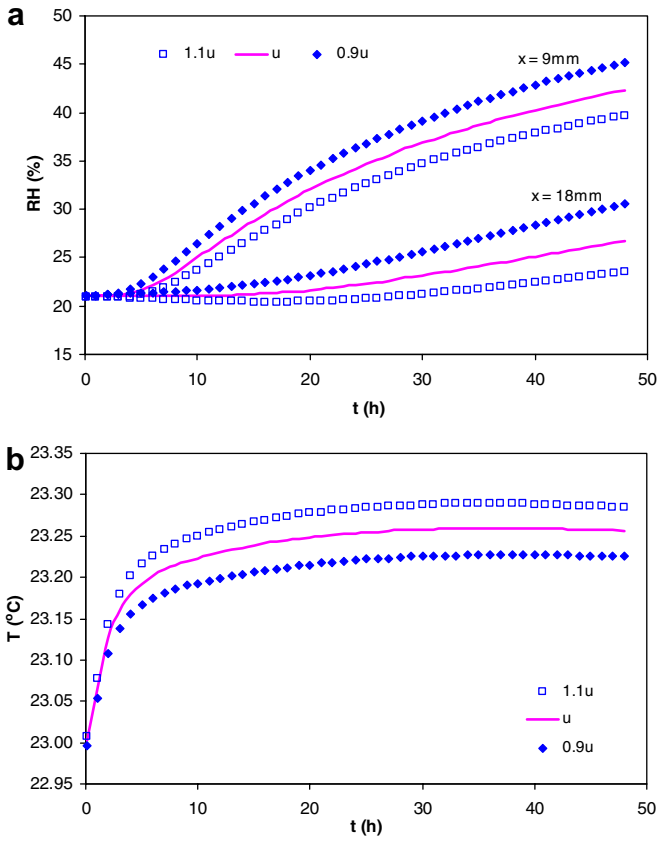

Fig. 7. Sensitivity study showing the effect of changing the moisture content (u) calculated by the sorption isotherm [1] by ±10% on the simulated (a) relative humidity and (b) temperature field within plywood at a depth of 9 mm following a 50% RH step change.

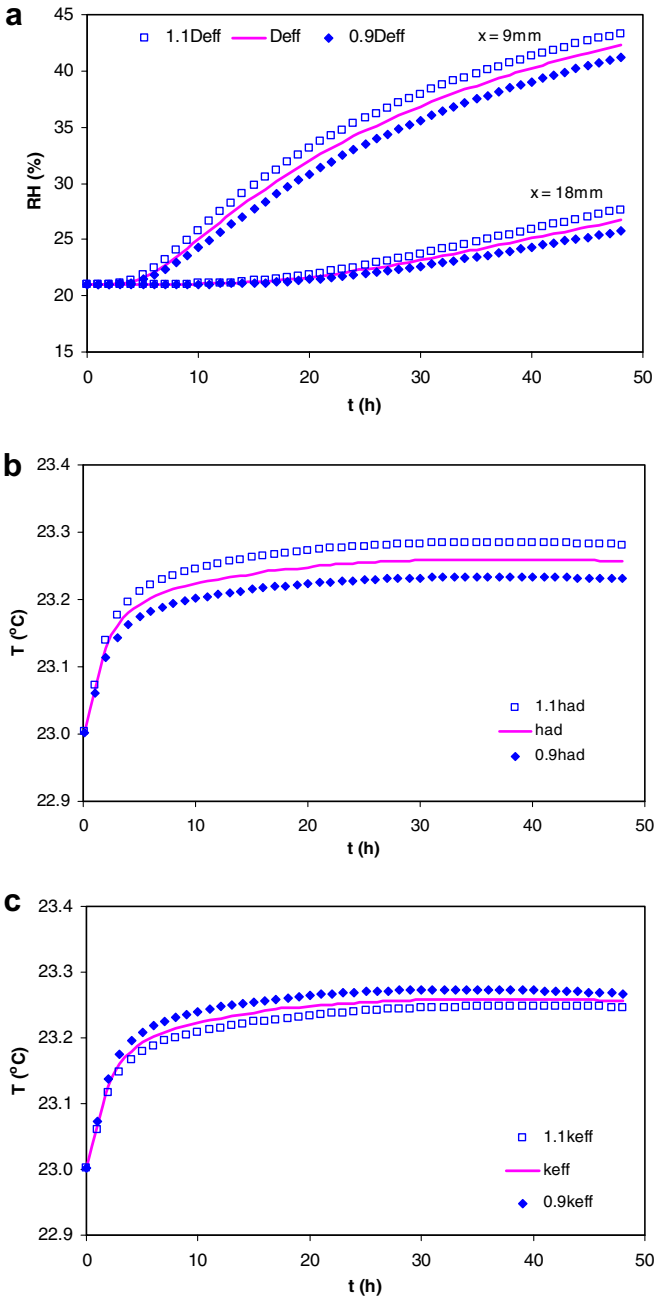

Fig. 8. Sensitivity study showing the effect of changing (a) D_{eff}, (b) h_{ad} and (c) k_{eff} [1] by ±10% on the simulated relative humidity and temperature of plywood at a depth of 9 mm following a 50% RH step change.

ically smaller than the fluctuations in Fig. 7a. Also, the differences between the measured and simulated temperatures shown previously (Figs. 1–6) are typically smaller than the fluctuations due to a ±10% change in the sorption curve.

The effective vapor diffusion coefficient (D_{eff}) is based on the water vapor permeability data presented in [1]. Increasing or decreasing D_{eff} by 10% results in a maximum of 2% increase or decrease in the humidity relative to the size of the step change in humidity (50%) as shown Fig. 8a. The numerical results show that increasing D_{eff} increases the relative humidity at all depths as expected. Changing D_{eff} by ±10% results in a ±4% change in the temperature (not presented graphically).

In the numerical simulation, the heat of sorption (h_{ad}) is assumed constant, while in reality the heat of sorption varies with moisture content, especially at low moisture contents [43]. This is accounted for in the simulation by increasing h_{ad} above the latent heat of vaporization of water (2.5×10^6 J/kg) for the cellulose which has a very dry initial condition ($\phi_i \approx 13\%$ RH). The value of h_{ad} used in the simulation of cellulose insulation and plywood is $h_{\text{ad}} = 3.25 \times 10^6$ J/kg and 2.5×10^6 J/kg respectively. As the property is not well quantified, it is important to investigate the effect of changes in h_{ad} on the simulated temperature. Increasing or decreasing h_{ad} by 10% in the numerical simulation results in a 8% maximum increase or decrease in temperature respectively as shown in Fig. 8b, but results in only a 0.1% decrease or increase respectively in the humidity (relative to the step size of 50% RH) and thus the results are not presented graphically. As expected, increasing h_{ad} increases the temperature field and thus decreases the relative humidity field, which demonstrates the coupling between the heat and moisture transport equations. The data in Fig. 8b show the influence of the heat of phase change on the expected results and provides a range of

acceptability when using this data for benchmarking a numerical model.

Changing the effective thermal conductivity by ±10% has a small effect (±3%) on the temperature field as shown in Fig. 8c and even smaller effect (±0.04%) on the humidity field relative to the size of the step change in humidity (50%) (not presented graphically). Fig. 8c shows that increasing k_{eff} tends to decrease the temperature in the spruce plywood because a higher value of k_{eff} results in more of the heat released during adsorption being conducted deeper into the plywood or upward through the plywood into the air stream. These results indicate that the model is correctly modeling the coupled heat and moisture transfer. They also confirm that the plywood is loosing heat to the ambient air during the test.

3. Analytical solution

Many engineering text books (e.g., [44]) contain solutions for transient conduction heat transfer problems and suggest that these solutions can be used for mass transfer as well, when analogous or equivalent moisture transfer properties are used in place of the heat transfer properties.

The effective moisture diffusivity of a porous media needs to include moisture storage [35,45] and the equation is

$$\alpha_{\text{m,eff}} = \frac{D_{\text{eff}}}{C_{\text{m}}}, \tag{1}$$

where

$$C_{\text{m}} = \left(\varepsilon_{\text{g}} + \frac{\rho_0 R_{\text{v}} T}{P_{\text{vsat}}} \frac{\partial u}{\partial \phi}\right). \tag{2}$$

The term $\frac{\partial u}{\partial \phi}$ is the slope of the sorption curve, where u is in kg/kg and ϕ is in fraction.

For the case of a semi-infinite porous medium with uniform initial conditions and constant properties subject to a step change in humidity of air above the medium, the analytical solution to the vapour transport equation is

$$\frac{\rho_{\text{v}} - \rho_{\text{vi}}}{\rho_{\infty} - \rho_{\text{vi}}} = \text{erfc}\left(\frac{x}{2\sqrt{\alpha_{\text{m,eff}} t}}\right) - \left[\exp\left(\frac{h_{\text{m}} x}{D_{\text{eff}}} + \frac{h_{\text{m}}^2 \alpha_{\text{m,eff}} t}{D_{\text{eff}}^2}\right)\right] \times \left[\text{erfc}\left(\frac{x}{2\sqrt{\alpha_{\text{m,eff}} t}} + \frac{h_{\text{m}}\sqrt{\alpha_{\text{m,eff}} t}}{D_{\text{eff}}}\right)\right]. \tag{3}$$

As the material properties (k_{eff}, D_{eff}, C_{m}, $\varepsilon_{\text{m,eff}}$, ρ) change with moisture content, average value of these properties over the test conditions ($\phi_{\text{i}} = 22\%$ RH, $\phi_{\infty} = 70\%$ RH, $T_{\infty} = 23\ ^{\circ}\text{C}$) are used in Eq. (3). This gives a value of $C_{\text{m}} = 1170$ for spruce plywood.

The moisture penetration depth (δ_{m}) is defined as the position in the porous medium where

$$\frac{\rho_{\text{v},\delta_{\text{m}}} - \rho_{\text{v,i}}}{\rho_{\infty} - \rho_{\text{v,i}}} = 0.01. \tag{4}$$

The moisture penetration depth (δ_{m}) can be calculated from the analytical, numerical and experimental data and these are presented in Fig. 9a. The experimental data are obtained by determining the time at which the measured relative humidity at $x = 9$ mm and $x = 18$ mm reaches 22.5% RH (which corresponds to $\rho_{\text{v},\delta_{\text{m}}} = 0.00464\ \text{kg/m}^3$) according Eq. (4). It takes 4.4 h and 19.1 h for the boundary layer to reach the sensors located at $x = 9$ mm and $x = 18$ mm respectively. The error bars in Fig. 9a represent the 95% uncertainty bounds in this measured time due to the precision uncertainty of the humidity sensors (±0.7% RH) as determined in part I [1]. This small precision uncertainty in relative humidity results in a reasonably large uncertainty in time because a small uncertainty in vapour density results in a large uncertainty in time due to the fact that the vapour density versus time graph has a very small slope at $\rho_{\text{v},\delta_{\text{m}}}$ as shown in Fig. 9b. The experimental uncertainties are ±1.5 h (±34%) and ±4.1 h (±21%) at $x = 9$ mm and $x = 18$ mm respectively. The uncertainty in the vertical location of the humidity sensors is less than ±0.5 mm and is not included in Fig. 9a. Fig. 9a shows reasonable agreement (within 3 mm or ±10%) between the simulated, experimental and analytical values of δ_{m} obtained using Eqs. (3) and (4). Similar good agreement between the analytical,

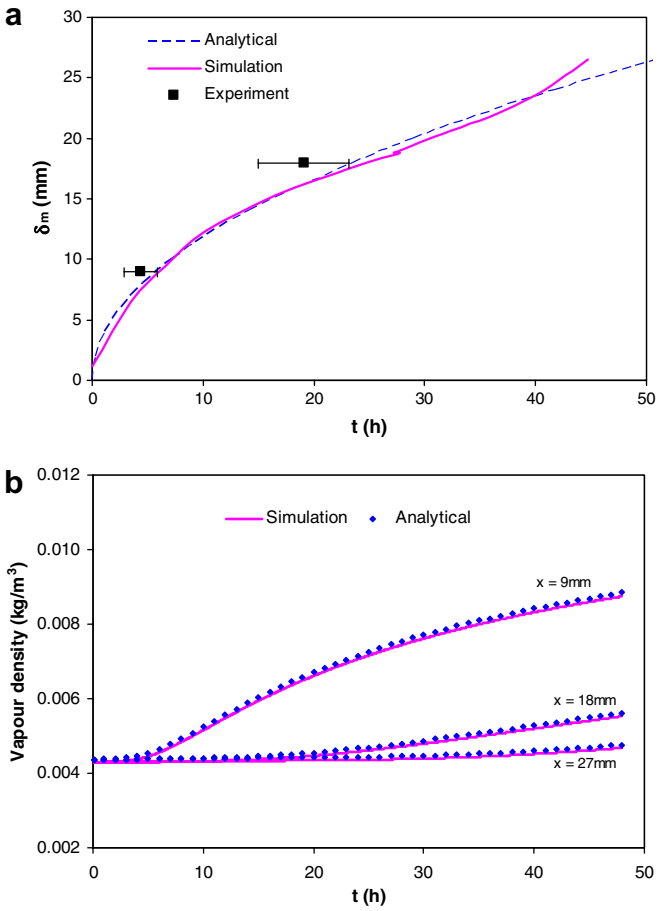

Fig. 9. (a) Vapor boundary layer thickness and (b) vapor density distribution in spruce plywood calculated using the analytical solution compared to that obtained from the numerical model and experimental data for $Re = 2000$.

experimental and numerical data for one test using cellulose is presented in [35] and is not repeated here.

Fig. 9b compares the vapor density within the porous medium calculated using analytical Eq. (3) with the simulated values. There is excellent agreement (within ±2%) between the analytical and simulated data.

4. Conclusions

This paper presents an experimental data set that quantifies the hygroscopic behaviour of two porous materials (spruce plywood and cellulose insulation). The data set includes the measured temperature and humidity at discrete points in the material as well as the average moisture content of the material. The measured data in this paper together with the material property data in Part I [1] and the data in [35] form a complete data set which can be used to benchmark 1-D transient models of heat and moisture transfer in hygroscopic building materials. This data set includes measurements over the following range of boundary conditions for the air flowing above the porous materials:

- air relative humidities from 15% RH to 85% RH,
- air temperatures of 20 °C and 38 °C,
- laminar and turbulent airflow (Reynolds numbers between 1000 and 7600),
- single and repeated step changes in air humidity, and
- test durations from 8 h to 12 days.

To ensure accuracy and increase creditability of the data set, the measured data are compared with numerical and analytical solutions. These comparisons together with the sensitivity studies presented in the paper provide the user of the data set with a indication of the reliability of the experimental data and a range of expected agreement when benchmarking numerical models.

Acknowledgements

The transient moisture transfer facility (TMT) that is described in this paper has been developed with funding from the Canada Foundation for Innovation (CFI), the Saskatchewan Innovation and Science Fund and the University of Saskatchewan. Funding for personnel is from the Natural Science & Engineering Research Council of Canada (NSERC) Discovery and Special Research Opportunity Programs. These financial contributions to the research are greatly appreciated.

Appendix. Mathematical model and boundary conditions

The 1-D conservation equations for mass and energy are the averaged transport equations over the representative elementary volume as listed below

$$\rho_l \frac{\partial \varepsilon_l}{\partial t} + \dot{m} = 0, \tag{A.1}$$

$$\frac{\partial(\rho_v \varepsilon_g)}{\partial t} - \dot{m} = \frac{\partial}{\partial x}\left(D_{eff}\frac{\partial \rho_v}{\partial x}\right), \tag{A.2}$$

$$\rho\, Cp_{eff}\frac{\partial T}{\partial t} + \dot{m} h_{fg} = \frac{\partial}{\partial x}\left(k_{eff}\frac{\partial T}{\partial x}\right). \tag{A.3}$$

The phase change rate ($\dot{m}$) can be determined from the rate of change of moisture content (u), which is obtained from the sorption isotherm

$$\dot{m} = -\rho_0 \frac{\partial u}{\partial t}, \tag{A.4}$$

where ρ_0 is the dry density and u is the moisture content.

The equations that quantify the changes in density and specific heat capacity due to changes in moisture content result from the local volume averaging of the governing equations and are

$$\rho = \varepsilon_s \rho_s + \varepsilon_g \rho_g + \varepsilon_l \rho_l, \quad \text{and} \tag{A.5}$$

$$Cp_{eff} = \frac{\varepsilon_s \rho_s Cp_s + \varepsilon_l \rho_l Cp_l + \varepsilon_g\{(\rho Cp)_a + (\rho Cp)_v\}}{\rho}. \tag{A.6}$$

Other equations required in the model for closure are as follows:

The volume constraint is

$$\varepsilon_s + \varepsilon_\ell + \varepsilon_g = 1. \tag{A.7}$$

The thermodynamic relationships are

$$P_v = \rho_v R_v T, \tag{A.8}$$

$$P_g = P_a + P_v, \tag{A.9}$$

$$P_a = \rho_a R_a T, \tag{A.10}$$

$$\rho_g = \rho_a + \rho_v, \tag{A.11}$$

$$\phi = \left.\frac{p_v}{P_{vsat}}\right|_T. \tag{A.12}$$

The saturation vapour pressure over liquid water is obtained from ASHRAE [46] as

$$P_{vsat} = \exp\left(\frac{C_1}{T} + C_2 + C_3 T + C_4 T^2 + C_5 T^3 + C_6 \ln T\right), \tag{A.13}$$

where $C_1 = -5.6745\text{E}+03$, $C_2 = 1.3915$, $C_3 = -4.8640\text{E}-02$, $C_4 = 4.1765\text{E}-05$, $C_5 = -1.4452\text{E}-08$, $C_6 = 6.5460$.

The boundary conditions for heat transfer are

$$h_a(T|_{x=0} - T_\infty) = k_{eff}\left.\frac{\partial T}{\partial x}\right|_{x=0}, \tag{A.14}$$

where

$$h_a = \frac{k_a Nu}{D_h}, \quad \text{and} \tag{A.15}$$

$$\left.\frac{\partial T}{\partial x}\right|_{x=L} = 0. \tag{A.16}$$

The boundary conditions for moisture transfer are

$$h_{\mathrm{m}}(\rho_{\mathrm{v}}|_{x=0} - \rho_{v,\infty}) = D_{\mathrm{eff}} \left.\frac{\partial \rho_{\mathrm{v}}}{\partial x}\right|_{\mathrm{x=0}}, \tag{A.17}$$

where

$$h_{\mathrm{m}} = \frac{D_{\mathrm{a}}\, Sh}{D_{\mathrm{h}}} \tag{A.18}$$

and

$$\left.\frac{\partial \rho_{\mathrm{v}}}{\partial x}\right|_{x=L} = 0. \tag{A.19}$$

References

[1] P. Talukdar, S.O. Olutmayin, O.F. Osanyintola, C.J. Simonson, An experimental data set for benchmarking 1-D, transient heat and moisture transfer models of hygroscopic building materials-Part-I: experimental facility and property data, Int. J. Heat Mass Transfer, in press, doi:10.1016/j.ijheatmasstransfer.2007.03.026.

[2] X. Lü, Modelling of heat and moisture transfer in buildings I. Model Program, Energy and Buildings 34 (2002) 1033–1043.

[3] S. Hameury, Moisture buffering capacity of heavy timber structures directly exposed to an indoor climate: a numerical study, Building and Environment 40 (2005) 1400–1412.

[4] J. Fan, X.Y. Cheng, X. Wen, W. Sun, An improved model of heat and moisture transfer with phase change and mobile condensates in fibrous insulation and comparison with experimental results, Int. J. Heat Mass Transfer 47 (2004) 2343–2352.

[5] N. Mendes, P.C. Philippi, A method for predicting heat and moisture through multilayered walls based on temperature and moisture content gradients, Int. J. Heat Mass Transfer 48 (2005) 37–51.

[6] J. Drchalová, R. Černý, A simple gravimetric method for determining the moisture diffusivity of building materials, Constr. Build. Mater. 17 (2003) 223–228.

[7] S.S. Kalagasidis, HAM-Tools-an integrated simulation tool for heat, air and moisture transfer analyses in building physics, Ph.D. thesis, Chalmers University of Technology, Goteborg, Sweden, 2004.

[8] C.J. Simonson, M. Salonvaara, T. Ojanen, Heat and mass transfer between indoor air and a permeable and hygroscopic building envelope, Part II – Verification and numerical studies, J. Therm. Envelope Build. Sci. 28 (2) (2004) 161–185.

[9] M. Izadifar, O-D. Baik, C.J. Simonson, Modeling of the packed bed drying of paddy rice using the local volume averaging (LVA) approach, Food Research International 39 (2006) 712–720.

[10] Q. Zhu, Y. Li, Effects of pore size distribution and fiber diameter on the coupled heat and liquid moisture transfer in porous textiles, Int. J. Heat Mass Transfer 46 (2003) 5099–5111.

[11] X. Luo, Q. Xu, A new numerical implementation on 2D heat and moisture transfer through fabric, Appl. Math. Comput, in press.

[12] B.C. Liu, W. Liu, S.W. Peng, Study of heat and moisture transfer in soil with a dry surface layer, Int. J. Heat Mass Transfer 48 (2005) 4579–4589.

[13] D.A. de Vries, The theory of heat and moisture transfer in porous media revisited, Int. J. Heat Mass Transfer 30 (1987) 1343–1350.

[14] L.Z. Zhang, J.L. Niu, Laminar fluid flow and mass transfer in a standard field and laboratory emission cell, Int. J. Heat Mass Transfer 46 (2003) 91–100.

[15] J. Fukai, Y. Hamada, Y. Morozumi, O. Miyatake, Improvement of thermal characteristics of latent heat thermal energy storage units using carbon-fiber brushes: experiments and modeling, Int. J. Heat Mass Transfer 46 (2003) 4513–4525.

[16] I. Dincer, M.M. Hussain, A.Z. Sahin, B.S. Yilbas, Developement of a new moisture transfer (Bi–Re) correlation for food drying applications, Int. J. Heat Mass Transfer 45 (2002) 1749–1755.

[17] M.M. Hussain, I. Dincer, Two-dimensional heat and moisture transfer analysis of a cylindrical moist object subjected to drying: A finite difference approach, Int. J. Heat Mass Transfer 46 (2003) 4033–4039.

[18] W.R. Foss, C.A. Bronkhorst, K.A. Bennett, Simultaneous heat and mass transport in paper sheets during moisture sorption from humid air, Int. J. Heat Mass Transfer 46 (2003) 2875–2886.

[19] J. Sun, R. Besant, Heat and mass transfer during silica gel-moisture interactions, Int. J. Heat Mass Transfer 48 (2005) 4953–4962.

[20] C.G. Jiang, M.Z. Saghir, M. Kawaji, K. Ghorayeb, Two-dimensional numerical simulation of thermo-gravitational convection in a vertical porous column filled with a binary fluid mixture, Int. J. Therm. Sci. 43 (2004) 1057–1065.

[21] Y. Ichikawa, G.L. England, Prediction of moisture migration and pore pressure build-up in concrete at high temperatures, Nucl. Eng. Des. 228 (2004) 245–259.

[22] C. Rode, M. Salonvaara, T. Ojanen, C.J. Simonson, K. Grau, Integrated hygrothermal analysis of ecological buildings, in: Research in Building Physics: Proceedings of the 2nd International Conference on Building Physics, Leuven, Belgium, September 14–18, 2003, pp. 859-868.

[23] N. Mendes, P.C. Philippi, R. Lamberts, A new mathematical method to solve highly coupled equations of heat and mass transfer in porous media, Int. J. Heat Mass Transfer 45 (2002) 509–518.

[24] M. Qin, R. Belarbi, A. Ait-Mokhtar, Alain Seigneurin, An analytical method to calculate the coupled heat and moisture transfer in building materials, Int. Commun. Heat Mass Transfer 33 (1) (2005) 39–48.

[25] J. Arfvidsson, M.J. Cunningham, A transient technique for determining diffusion coefficients in hygroscopic materials, Build. Environ. 35 (2000) 239–249.

[26] S. Roles, J. Carmeliet, H. Hens, O. Adan, H. Brocken, R. Cerny, Z. Pavlik, C. Hall, K. Kumaran, L. Pel, R. Plagge, Interlaboratory comparison of hygric properties of porous building materials, J. Therm. Envelope Build. Sci. 27 (4) (2004) 307–325.

[27] C.J. Simonson, M. Salonvaara, T. Ojanen, The effect of structures on indoor humidity – possibility to improve comfort and perceived air quality, Indoor Air 12 (2002) 243–251.

[28] A.H. Holm, H.M. Kuenzel, K. Sedlbauer, Predicting indoor temperature and humidity conditions including hygrothermal interactions with the building envelope, ASHRAE Trans. 110 (2) (2004) 820–826.

[29] C.J. Simonson, M. Salonvaara, T. Ojanen, Moderating indoor conditions with hygroscopic building materials and outdoor ventilation, ASHRAE Trans. 110 (2) (2004) 804–819.

[30] C.J. Simonson, Y-X. Tao, R.W. Besant, Simultaneous heat and moisture transfer in fibreglass insulation with transient boundary conditions, ASHRAE Trans. 102 (1) (1996) 315–327.

[31] C.J. Simonson, M. Salonvaara, T. Ojanen, Heat and mass transfer between indoor air and a permeable and hygroscopic building envelope, Part I – Field Measurements, J. Therm. Envelope Build. Sci. 28 (1) (2004) 63–101.

[32] C.J. Simonson, T. Ojanen, M. Solonvaara, Moisture performance of an airtight vapour permeable building envelope in a cold climate, J. Therm. Envelope Build. Sci. 28 (3) (2005) 205–226.

[33] N.E. Wijeysundera, M.N.A. Hawlader, Effect of condensation and liquid transport on the thermal performance of fibrous insulation, Int. J. Heat Mass Transfer 35 (1992) 2605–2616.

[34] N.E. Wijeysundera, B.F. Zheng, Numerical simulation of the transient moisture transfer through porous insulation, Int. J. Heat Mass Transfer 39 (1995) 995–1003.

[35] S. Olutimayin, C. Simonson, Measuring and modelling vapor boundary layer growth during transient diffusion heat and moisture transfer in cellulose insulation, Int. J. Heat Mass Transfer 48 (2005) 3319–3330.

[36] O.F. Osanyintola, P. Talukdar, C.J. Simonson, Effect of initial conditions boundary conditions and thickness on the moisture buffering capacity of spruce plywood, Energy Buildings 38 (2006) 1283–1292.

[37] C.-E. Hagentoft, A.S. Kalagasidis, B. Adl-Zarrabi, S. Roels, J. Carmeliet, H. Hens, J. Grunewald, M. Funk, R. Becker, D. Shamir,

O. Adan, H. Brocken, K. Kumaran, R. Djebbar, Assessment method of numerical prediction models for combined heat air and moisture transfer in building components: benchmarks for one-dimensional cases, J. Therm. Envelope Build. Sci. 27 (2004) 327–352.

[38] H.M. Kuenzel, Simultaneous Heat and Mositure Transport in Building Components one-and two-dimensional calculation using simple parameters, IRB Verlag, Fraunhofer-Institut fur bauphysik, Stuttgart, Germany, 2005.

[39] P. Mukhopadhyaya, M.K. Kumaran, J.C. Lackey, J.C, Use of the modified cup method to determine temperature dependency of water vapor transmission properties of building materials, J. Test. Evaluat. 33 (2005) 316–322.

[40] O.F. Osanyintola, Transient moisture characteristics of spruce plywood, M.Sc. thesis, Department of Mechanical Engineering, University of Saskatchewan, Saskatoon, SK, Canada, 2005, http://library.usask.ca/theses/available/etd-12222005-082100.

[41] S.O. Olutimayin, Vapor boundary layer growth during transient heat and moisture transfer in cellulose insulation, M.Sc. thesis, Department of Mechanical Engineering, University of Saskatchewan, Saskatoon, SK, Canada, 2004.

[42] Skogstad, H.B., Abell, P., Jonsson, B. and Simonson, C.J., Equipment for measuring thermal resistance-Intercalibration, Final report of Nordtest project 1488-00, Norwegian Building Research Institute, Trondheim, 9 pages, January, 2001.

[43] Y.X. Tao, R.W. Besant, C.J. Simonson, Measurement of the heat of adsorption for a typical fibrous insulation, ASHRAE Trans. 98 (2) (1992) 495–501.

[44] F.P. Incropera, D.P. Dewitt, Fundamentals of Heat and Mass Transfer, John Wiley & Sons, New York, 2001.

[45] IEA, Source Book, Final Report, Vol 1, IEA ECBCS Annex 14, 1991.

[46] ASHRAE, Fundamentals Handbook, Atlanta, GA, USA, 2005.

[47] C.R. Ickra, C.J. Simonson, Convective mass transfer coefficient for a hydrodynamically developed airflow in a short rectangular duct, Int. J. Heat Mass Transfer 50 (2007) 2376–2393.

[48] L.H. Mortensen, M. Woloszyn, C. Rode, R. Peuhkuri, Investigation of microclimate by CFD modeling of moisture interactions between air and constructions, J. Build. Phys. 30 (2007) 279–315.